How to cite: *Angew. Chem. Int. Ed.* **2022,** *61,* e202207300
International Edition: doi.org/10.1002/anie.202207300
German Edition: doi.org/10.1002/ange.202207300

Fluorescent Quantum Dots

Suppressing Non-Radiative Relaxation through Single-Atom Metal Modification for Enhanced Fluorescence Efficiency in Molybdenum Disulfide Quantum Dots

Chao-Rui Li[+], Yu-Li Lei[+], Hua Li[+], Miao Ni, Dong-Rui Yang, Xiao-Yu Xie, Yuan-Fan Wang, Hai-Bo Ma, Wei-Gao Xu,* and Xing-Hua Xia**

Abstract: To enhance the fluorescence efficiency of semiconductor nanocrystal quantum dots (QDs), strategies via enhancing photo-absorption and eliminating non-radiative relaxation have been proposed. In this study, we demonstrate that fluorescence efficiency of molybdenum disulfide quantum dots (MoS_2 QDs) can be enhanced by single-atom metal (Au, Ag, Pt, Cu) modification. Four-fold enhancement of the fluorescence emission of MoS_2 QDs is observed with single-atom Au modification. The underlying mechanism is ascribed to the passivation of non-radiative surface states owing to the new defect energy level of Au in the forbidden band that can trap excess electrons in n-type MoS_2, increasing the recombination probability of conduction band electrons with valence band holes of MoS_2. Our results open an avenue for enhancing the fluorescence efficiency of QDs via the modification of atomically dispersed metals, and extend their scopes and potentials in a fundamental way for economic efficiency and stability of single-atom metals.

As a kind of common semiconductor nanocrystal regarded as zero-dimensional nanomaterials, quantum dots (QDs) exhibit various unique characteristics of strong quantum confinement and edge effect,[1] noticeable quantum-size effect[2] and large Stokes shift,[3] showing potential applications in various fields of optoelectronic devices, photoelectrocatalysis and bioimaging.[4] To date, various strategies have been proposed to enhance the luminescence efficiency of the existing QDs via increasing photo-absorption[5] and eliminating non-radiative relaxation.[6,7] QDs emit fluorescence through the exciton-recombination process of the conduction band electrons with holes at the valence band.[8,9] Thus, the number of photons can be increased by enhanced photo-absorption,[10,11] and the acceleration of radiative recombination of luminescence can be achieved by suppressing the non-radiative relaxation processes like thermal dissipation and vibration relaxation.[12–14] Experimentally, these strategies to enhance the luminescence efficiency can be achieved by regulating the electronic structure of the phosphor via modification of structure and surface states.[15,16] However, conventional approaches commonly suffer from their expensive cost and uncontrollability,[17–19] and it is usually hard to establish a precise structure–functionality relationship at the atomic level. Thus, development of novel and simple strategies to modulate the electronic structure of QDs for obtaining phosphors with high luminescence efficiency is still highly desired.

The recently developed atomically dispersed metals supported on various matrices have attracted broad interest in fundamental research and practical applications. They maximize the efficiency of atomic utilization, and significantly change their physical and chemical properties via electronic interactions between the single-atom metals and the substrates.[20,21] The utilization of single-atom metal modification as high performance catalysts has been described in recent reviews.[22,23] Recently, Wang and coworkers[24] reported that atomically dispersed Ni in zinc-blende cadmium-zinc sulfide quantum dots exhibited an efficient and durable photocatalytic performance for hydrogen production. They ascribed the improved photocatalytic performance to the highly active sites of monovalent Ni^{I} and the high carrier separation. Hence, owing to the economic efficiency and stability of single-atom metals, their modification can be expected to be also an ideal strategy candidate to precisely regulate the fluorescence emission properties of phosphors through the modulation of their electronic surroundings.[25,26]

Here, we report the enhanced fluorescence efficiency of molybdenum disulfide quantum dots (MoS_2 QDs) via atomically dispersed metals modification. Monolayer or bilayer MoS_2 QDs are synthesized by a one-step exfoliation using ethylenediamine followed by calcination at 130 °C (see Experimental in Supporting Information). Single-atom metal modification of the QDs ($^{s}M/MoS_2$ QDs, M = Au, Ag, Pt and Cu) is achieved by underpotential deposition (UPD) of

[*] Dr. C.-R. Li,[+] M. Ni, Dr. D.-R. Yang, Prof. X.-H. Xia
State Key Laboratory of Analytical Chemistry for Life Science, School of Chemistry and Chemical Engineering, Nanjing University
Nanjing 210023 (P. R. China)
E-mail: xhxia@nju.edu.cn
Y.-L. Lei,[+] Dr. H. Li,[+] Dr. X.-Y. Xie, Y.-F. Wang, Prof. H.-B. Ma, Prof. W.-G. Xu
Key Laboratory of Mesoscopic Chemistry of MOE, School of Chemistry and Chemical Engineering, Nanjing University
Nanjing 210023 (P. R. China)
E-mail: haibo@nju.edu.cn
xuwg@nju.edu.cn
[+] These authors contributed equally to this work.

copper atoms on QDs followed by galvanic replacement.[27] We find that the $^{s}M/MoS_2$ QDs exhibit enhanced fluorescence efficiency of MoS_2 QDs with up to a four-fold increase for the Au modification. This phenomenon is ascribed to the passivation of non-radiative surface states caused by the new defect energy level of single-atom metals in the forbidden band that traps extra electrons in n-type MoS_2, which increases the possibilities for the recombination of conduction band electrons with valence band holes of MoS_2.

The stable and luminescent MoS_2 QD was selected as an ideal phosphor substrate for single-atom metal modification. We designed an approach to synthesize MoS_2 QDs by intercalating ethylenediamine into the interlayers of MoS_2 sheets, followed by ultrasonic exfoliation and subsequently calcination at 130 °C (Scheme S1). The high-resolution transmission electron microscopy (HRTEM) image in Figure S1a shows that the synthesized MoS_2 QDs have polydisperse and uniform small wafer shape with an average diameter of ≈3.8 nm. They have a well-defined lattice fringe with highly ordered parallel lines as displayed by the magnified HRTEM image of a single quantum dot (Figure 1a). The lattice spacing is 0.23 nm, corresponding well to the (103) plane of MoS_2 QDs.[28] The single MoS_2 QD has a height of ≈2.1 nm as revealed by the atomic force microscopy (AFM) image (Figure S2), suggesting a monolayer or bilayer structure.[29]

Single-atom Cu was then deposited on the MoS_2 QDs through an UPD technique at a constant deposition potential of 0.150 V vs. Ag/AgCl/KCl (3.0 M), forming $^{s}Cu/MoS_2$ QDs (Figure S3). The single-atom Cu was then galvanically replaced by using metallic precursors to form single-atom metals (Au, Ag or Pt) on MoS_2 QDs (Scheme S2).[27,30,31] The single-atom metal modification procedure retains the morphology and dispersion of MoS_2 QDs as revealed by the HRTEM images (Figures 1b and S1). The high-angle annular dark field-scanning transmission electron microscopic (HAADF-STEM) images of $^{s}Au/MoS_2$ QDs, $^{s}Ag/MoS_2$ QDs and $^{s}Pt/MoS_2$ QDs clearly demonstrate the uniform dispersion of individual Au, Ag or Pt atoms anchored on the surface of single MoS_2 QDs, and the morphology and lattice fringe of MoS_2 QDs are retained (Figures 1c and S4).

The chemical compositions and properties of MoS_2 QDs and $^{s}M/MoS_2$ QDs were explored by conducting X-ray photoelectron spectroscopy (XPS), and the results are shown in Figures 1d–f and S5–S9. The survey spectrum of MoS_2 QDs (Figure S5) exhibits several significant signals at 164, 228, 285, 399 and 531 eV, which are attributed to S (2*p*), Mo (3*d*), C (1*s*), N (1*s*) and O (1*s*), respectively.[32] The high-resolution XPS spectra display that the binding energies of Mo^{4+} ($3d_{5/2}$) and Mo^{4+} ($3d_{3/2}$) are 228.0 and 231.6 eV, while those of S^{2-} ($2p_{1/2}$) and S^{2-} ($2p_{3/2}$) are 164.1 and 167.3 eV, respectively. After single-atom Au modification, there exists only a band for Mo^{4+} (3*d*) and S^{2-} (2*p*) located at higher

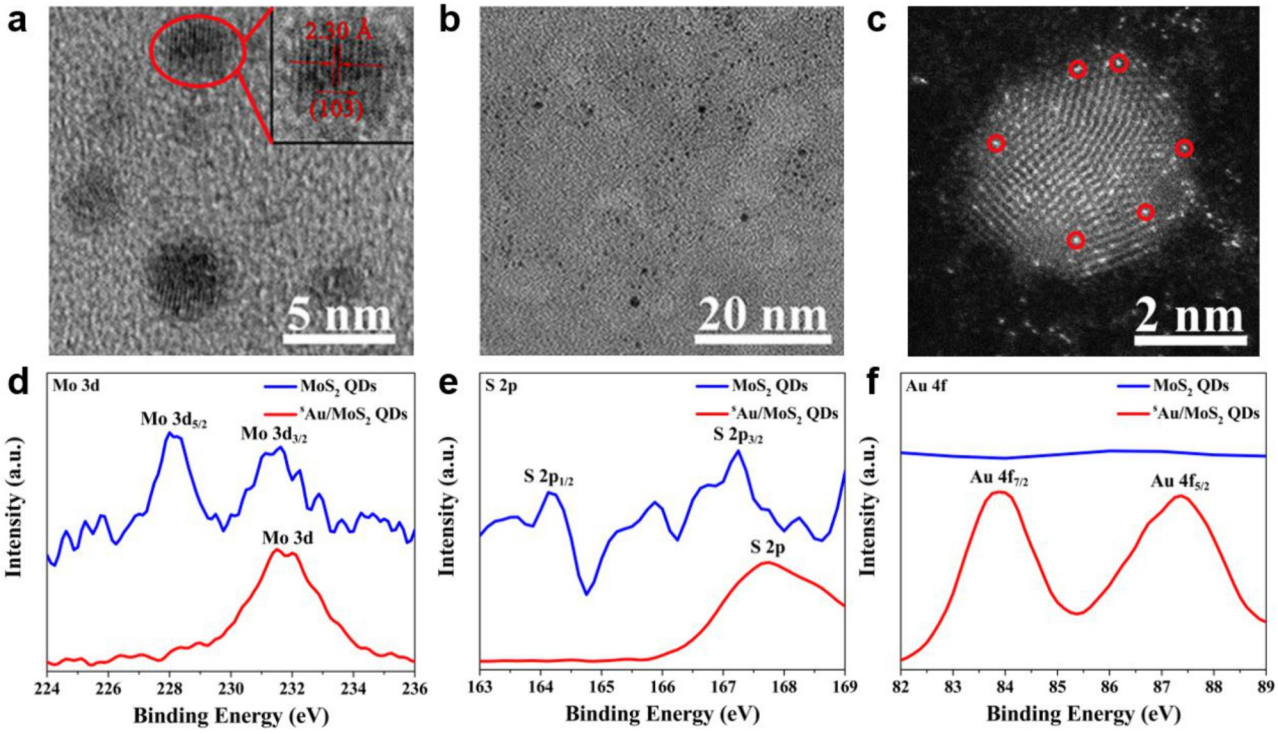

Figure 1. Characterizations of $^{s}Au/MoS_2$ QDs. a) HRTEM image of MoS_2 QDs (scale bar, 5 nm). The inset presents the amplified HRTEM image of a single MoS_2 QD outlined with a red circle. b) HRTEM image of $^{s}Au/MoS_2$ QDs (scale bar, 20 nm). c) HAADF-STEM image of $^{s}Au/MoS_2$ QDs (scale bar, 2 nm). Individual Au atoms are outlined by red circles. High-resolution XPS spectra of MoS_2 QDs and $^{s}Au/MoS_2$ QDs corresponding to Mo 3*d* (d), S 2*p* (e) and Au 4*f* (f).

binding energies of 232.0 and 167.8 eV (Figures 1d, e), respectively. These phenomena could be due to the transfer of partial electrons from S^{2-} in MoS_2 QDs to single-atom Au, inducing a decrease in the electronic density in the 3*d* orbital of Mo^{4+} and 2*p* orbital of S^{2-} of MoS_2 due to the electron transfer from Mo^{4+} to S^{2-} to maintain the electric neutrality of the Mo–S bond. The appearance of only one band for Mo 3*d* or S 2*p* might be due to the decreased splitting energies of the spin orbitals of Mo^{4+} (3*d*) and S^{2-} (2*p*) caused by electron transfer.[33] The characteristic signals at 84.0 and 87.4 eV of $^{s}Au/MoS_2$ QDs are assigned to Au ($4f_{7/2}$) and Au ($4f_{5/2}$) energy levels, respectively (Figure 1f),[34] proving the successful modification of Au on MoS_2 QDs. The observed N (1*s*) signal originates from some residual ethylenediamine molecules absorbed on MoS_2 QDs. Its binding energy shifts to a higher value (401 eV) upon modification of single-atom Au (Figure S6a), indicating partial electron transfer from the ethylenediamine molecules to $^{s}Au/MoS_2$ QDs. Similar changes in the XPS spectra are also visualized with the modification of single-atom Ag, Pt or Cu on MoS_2 QDs (Figures S6–S9),[35–37] indicating the similar electron transfer process from MoS_2 to single-atom metals.

The UV/Vis absorption spectra (Figure S10) of MoS_2 QDs and $^{s}M/MoS_2$ QDs were tested for characterizing their electronic structures. The MoS_2 QDs suspension exhibits two distinct absorption bands centered at 266 nm and 328 nm attributed to the excitonic performance of MoS_2 QDs and an extremely small shoulder band at around 380 nm.[38] Negligible changes in the spectra are observed with the modification of single-atom Au, Ag, Pt or Cu. In addition, the characteristic absorption bands of the corresponding metallic nanoclusters, which should occur at above 400 nm, are not observed (Figure S10),[39–42] demonstrating the absence of metallic nanoclusters or nanoparticles in these systems. In the photoluminescence excitation (PLE) spectrum of MoS_2 QDs, a fluorescence emission peak at 460 nm appears at the excitation peak (382 nm), which is in line with its shoulder band in the UV/Vis absorption, indicating an optimal excitation wavelength of 382 nm. The relatively broad PLE spectrum suggests that pure MoS_2 QDs can be photoexcited over a broad wavelength (Figure S11).

The fluorescence emission spectra of pure MoS_2 QDs under excitation at different wavelengths show the strongest band centered at 460 nm upon excitation at 382 nm (Figure S12), which is correlated to the surface states of MoS_2 QDs, proving the superior excitation wavelength of 382 nm for measuring the fluorescence emission spectrum of MoS_2 QDs (Figure S11). We confirm that the fluorescence emission originates from MoS_2 QDs rather than from solvent or residual ethylenediamine molecules, as indicated by the control experiments (Figure S13). The relatively broadened emission band of MoS_2 QDs is probably due to their size distribution originating from the quantum-size effect.[2] The fluorescence emission spectra of MoS_2 QDs are hardly altered when retained for 6 months at ambient temperature and under illumination by a 365 nm UV lamp for 90 min (Figure S14), proving the excellent chemical stability and photostability of MoS_2 QDs. In addition, the fluorescence emission intensity at 460 nm (Figure S15) shows a suspension pH independence in the range of 0–13. However, it starts to decrease at a pH higher than 14, which could be due to aggregation of MoS_2 QDs caused by excessive OH^-, leading to self-quenching.[43] These results demonstrate that MoS_2 QDs display high chemical stability, photostability and anti-interference against pH.

The fluorescence emission spectra of $^{s}M/MoS_2$ QDs conducted under the same conditions of MoS_2 QDs in pure water with excitation at 382 nm are shown in Figure 2a. The $^{s}M/MoS_2$ QDs exhibit a fluorescence emission band at 460 nm, stronger than the as-synthesized MoS_2 QDs with their intensities enhanced by 4.00, 2.45, 2.29 and 1.68-fold for ^{s}Au, ^{s}Ag, ^{s}Pt and ^{s}Cu, respectively (Figure 2a). The results demonstrate that single-atom metal modification changes the fluorescent property of MoS_2 QDs. We prove that the fluorescence emission enhancement of MoS_2 QDs is attributed to the atomically dispersed metals modification, but not to the possible existence of metallic precursors in the suspension (Figure S16). Our control experiments display decreased band intensity of the fluorescence emission at 460 nm upon respective addition of metallic precursors (Au^{3+}, Ag^+, Pt^{2+} or Cu^{2+}), which is attributed to the electron and energy transfer processes from the photo-induced metallic cations to MoS_2 QDs.[44] Thus, we assume that the single-atom metal modification enhanced fluorescence emission is probably due to the introduction of a new defect energy level in the forbidden band of MoS_2 QDs, and this level serves as a deep impurity, which can trap excess electrons in n-type MoS_2,[45,46] passivating multi-particle non-radiative surface states,[47] and thus increasing the radiative recombination efficiency to enhance the fluorescence emission.[48] Transient fluorescence measurements show a slight decrease in fluorescence lifetime at 460 nm upon single-atom metal modification (Figures 2c, S17 and Table S1), which is probably attributed to the fact that the non-radiative dissipation from the defect energy level to valence band of MoS_2 is a little faster than the exciton radiation process.[49] The more obvious enhancement observed in $^{s}Au/MoS_2$ QDs compared with other $^{s}M/MoS_2$ QDs can be visualized by the best matched degenerate electron energy of the 5*d* atomic orbital of ^{s}Au with the 3*p* atomic orbital of S (Figures 2b, S18 and Table S2), which is calculated from the orbital number divided by the sum of each electron energy originating from density functional theory (DFT) calculations, and the best match favors the electron transfer from MoS_2 QDs to ^{s}Au. The enhanced fluorescence efficiency is significantly decreased on increasing the density of Au atoms on MoS_2 QDs (Figure S19), as indicated by the control experiment of Au nanoclusters modified MoS_2 QDs (Au NCs/MoS_2 QDs) (Figure S20) synthesized by using a method similar to that for $^{s}Au/MoS_2$ QDs except that the deposition potential was set at −0.200 V.[50] The fluorescence emission enhancement of MoS_2 QDs by single-atom Au modification is also observed from the fluorescence spectra of individual QDs at 395 nm excitation (Figures 2d and S21). The $^{s}Au/MoS_2$ QD shows the stronger PL intensity with a slight red-shift compared to

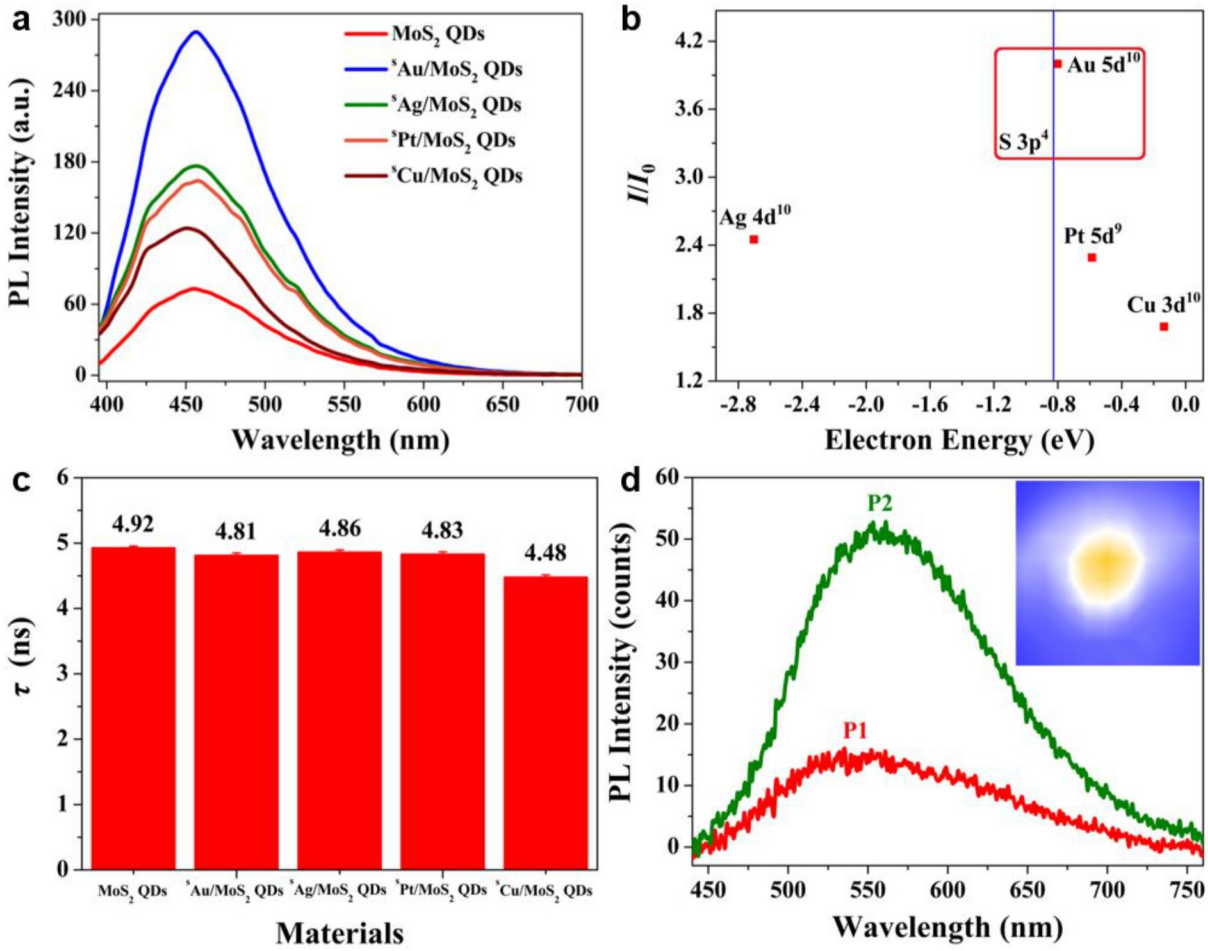

Figure 2. Fluorescence efficiency enhancement of MoS_2 QDs via single-atom metal modification. a) Fluorescence emission spectra of MoS_2 QDs, $^{s}Au/MoS_2$ QDs, $^{s}Ag/MoS_2$ QDs, $^{s}Pt/MoS_2$ QDs and $^{s}Cu/MoS_2$ QDs with the same concentration of 13.17 mg mL^{-1} in ultrapure water (λ_{ex} = 382 nm). b) Enhancement factor in fluorescence emission intensity at 460 nm (I/I_0) of MoS_2 QDs (13.17 mg mL^{-1}) with the modification of ^{s}Au, ^{s}Ag, ^{s}Pt or ^{s}Cu as a function of the calculated electron energy of their *d* atomic orbitals. The vertical axis represents the ratio between fluorescence emission intensity at 460 nm of $^{s}M/MoS_2$ QDs and MoS_2 QDs, and the horizontal axis represents the degenerate electron energy of Au 5*d*, Ag 4*d*, Pt 5*d*, Cu 3*d* and S 3*p* atomic orbitals calculated from the orbital number divided by the sum of each electron energy. The highest enhancement factor for ^{s}Au is due to the matched 5*d* atomic orbital energy with the 3*p* atomic orbital of S that favors electron transfer. c) Bar graph representing the fluorescence lifetime τ at 460 nm of MoS_2 QDs, $^{s}Au/MoS_2$ QDs, $^{s}Ag/MoS_2$ QDs, $^{s}Pt/MoS_2$ QDs and $^{s}Cu/MoS_2$ QDs with the same concentration of 13.17 mg mL^{-1} in ultrapure water (λ_{ex} = 382 nm). d) Fluorescence emission spectra of an individual MoS_2 QD (P1) and an individual $^{s}Au/MoS_2$ QD (P2) in Figure S21. The inset presents the fluorescence emission spectrometry mapping of an individual $^{s}Au/MoS_2$ QD (P2) in Figure S21 (λ_{ex} = 395 nm).

the MoS_2 QD. The averaged fluorescence gray value of individual $^{s}Au/MoS_2$ QDs is around four-fold that of MoS_2 QDs (Figure S22), which is in good agreement with the results in aqueous suspension. The above results elucidate that the single-atom Au modification shows the best performance for enhancing the fluorescence efficiency of MoS_2 QDs and thus, the strongest fluorescence emission at 460 nm of $^{s}Au/MoS_2$ QDs is observed upon excitation at 382 nm, which is similar to the results of other $^{s}M/MoS_2$ QDs (Figure S23).

We took the single-atom Au modification as an example to explore the fluorescence enhancement mechanism of MoS_2 QDs by DFT calculations. Since the acquisition of simulated structures for monolayer MoS_2 QDs and $^{s}Au/MoS_2$ QDs is troublesome due to their small wafer-shaped morphology with the average diameter of ≈3.8 nm (Figures 1, S1 and S2), we utilized a MoS_2 nanosheet with a monolayer thickness to reflect the monolayer MoS_2 QDs for establishing the structural models for simplicity. Three possible structural models for the ^{s}Au/monolayer MoS_2 nanosheet after DFT geometry optimizations are illustrated in Figures 3a, S24a and S25a, which are respectively defined as the configuration of Au–S, Au–Mo and Au–3S. The Au–S configuration is the most energy-favorable structural model for its lowest free energy (E_{QD}) of −558.35 eV (Table S3), the lowest binding energy (E_{comb}) of −1.11 eV (Table S3), and more homogeneous overall charge distributions (Figure 3b) compared to the other two structural models.[51] The qualitative charge distributions of these three simulated structural models for ^{s}Au/monolayer MoS_2 nano-

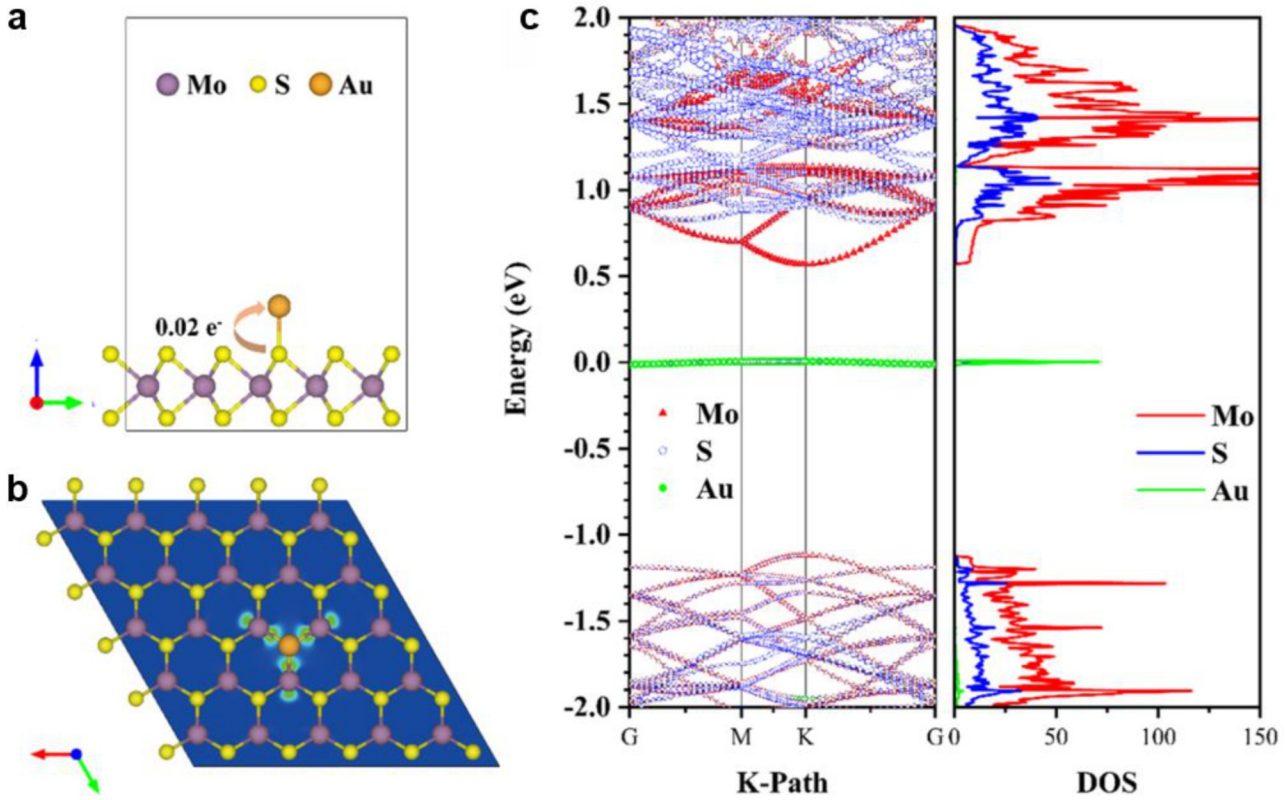

Figure 3. Mechanism on fluorescence efficiency enhancement of MoS_2 QDs via single-atom Au modification. a) DFT-optimized structural model with side view simulated for Au–S configuration of ^{s}Au/monolayer MoS_2 nanosheet. The Au atom is located on the top of one S atom and is coordinated with the adjacent S atoms to form Au–S bonds, along with the electron transfer from MoS_2 to Au. b) Charge transfer map of Au–S configuration of ^{s}Au/monolayer MoS_2 nanosheet showing a higher electron concentration around Au atoms (blue surface) and higher hole concentration around Mo atoms far away from Au–S bonds (yellow surface), indicating the p-type doping of Au to cause the transfer of partial electrons from S^{2-} in MoS_2 to single-atom Au, which induces a decrease in the electronic density in the 3*d* orbital of Mo^{4+} and 2*p* orbital of S^{2-} of MoS_2 due to the electron transfer from Mo^{4+} to S^{2-} to maintain the electric neutrality of the Mo–S bond. c) Electronic band structure and density of state (DOS) as a function of energy in levels of Au–S configuration of ^{s}Au/monolayer MoS_2 nanosheet showing the conduction band and valence band. Note that the Fermi energy has been set to zero and DFT calculations do not consider the spin-orbital coupling. The fluorescence enhancement mechanism is ascribed to the introduction of a new deep-level state (p-type doping) of Au serving as a trapping center to decrease the electron concentration in n-type MoS_2, which passivates non-radiative multi-electron surface states, and thus increases the recombination probability of conduction band electrons with valence band holes of MoS_2.

sheet were analyzed to characterize the electron transfer. From the charge transfer maps of these three models shown in Figures 3b, S24b and S25b, we can clearly observe a higher electron concentration around Au atoms and higher hole concentration around Mo atoms far away from Au–S bonds, demonstrating a strong tendency of transferring electrons from MoS_2 to Au atoms (e.g. 0.02 e^- transferred from MoS_2 to Au in the Au–S model, Figure 3a), which is also in good agreement with our experimental results of XPS studies. The change in the charge distributions induced by a single-atom Au modification might be recognized as the p-type doping,[52] which would contribute to the fluorescence efficiency enhancement.

DFT calculations demonstrate that MoS_2 has an energy band gap of ≈1.7 eV between the conduction and valence bands. This energy band gap and the feature of direct gap semiconductor of MoS_2 are not changed after single-atom Au modification (Figures 3c and S26), thus, similar fluorescence emission wavelengths are expected to be observed for these two systems, in accordance with our experimental findings (Figure 2a). However, a new defect energy level (p-type doping effect) is introduced in the forbidden band of MoS_2 owing to the single-atom Au modification,[52] which is expected to show a strong localization demonstrated by the weak band dispersion (Figure 3c). Hence, we suggest that the enhanced fluorescence emission originates from the deep-level defect state of Au, which is able to trap extra electrons from the conduction band of n-type MoS_2,[45,46] thus passivating non-radiative multi-electron surface states,[47] which contributes to higher possibilities for the recombination of conduction band electrons with valence band holes[48] and accordingly increases the fluorescence efficiency (Figures 3 and S26). The rate of the trapping process is higher than that of non-radiative relaxations, resulting in the increase of emission intensity as well as the slight variations of absorption and fluorescence lifetime (Figures 2a,c, S10, S17 and Table S1). Thus, the radiative recombination of luminescence rather

than the number of photons plays a conclusive role in the fluorescence efficiency enhancement. Interestingly, the doping of Ag, Pt and Cu shows the similar fluorescence efficiency enhancement of MoS_2 QDs without changes in the energy band gap, however, the unsuitable positions of the defect energy levels limit their enhancement to some extents (Figures S27–S29). These results further demonstrate that single-atom Au modification shows the significant fluorescence efficiency enhancement of MoS_2 QDs (Figure 2a). Similar phenomena are obtained in the calculated density of states (DOSs) and electronic band structures of another two structural models (Figures S24c and S25c), which confirms the validity of our assumption.

The above enhancement mechanism of fluorescence efficiency of MoS_2 QDs upon single-atom metal modification indicates its importance in causing the p-type doping effect. This p-type doping could be inhibited by increasing the electronic state density of the modified single-atom metal, e.g., the single-atom metal coordinates to an electron donor such as L-cysteine (L-Cys). We used $^{s}Au/MoS_2$ QDs as models to demonstrate how the L-Cys coordination to Au affects their fluorescence efficiency. When L-Cys is coordinated to the modified single-atom Au in $^{s}Au/MoS_2$ QDs, the fluorescence emission at 460 nm is decreased by 27.50 % (Figure S30a). To understand this phenomenon, we conducted Hirshfeld quantitative charge analysis[53] for the elaborated three structural models of ^{s}Au/monolayer MoS_2 nanosheet with adsorption of L-Cys. In these structural modes, calculation results show that the electron transfer from MoS_2 QDs to single-atom Au decreases from 0.18 e^- to −0.03 e^- at most (Figure S31, S32 and Table S4), resulting in a decreased electron density around Au, which can be transferred to the conduction band of n-type MoS_2, so the trapping process is restricted, which activates the multi-particle non-radiative surface states,[47] and thus decreases the radiative recombination efficiency of electrons with holes.[48] In addition, the fluorescence lifetime is increased from 4.81 ns to 4.95 ns (Figure S30b and Table S1) upon L-Cys coordination, probably caused by the prolonged non-radiative dissipation from the defect energy level of Au to the valence band of MoS_2.[49] The preferred coordination of L-Cys with Au is further proven by the lowest values of E_{QD} (−635.62 eV) and E_{comb} (−1.78 eV) (Figure S33 and Table S5) in this structural model with a Au–S–L-Cys coordination site.

In summary, we have demonstrated that the fluorescence efficiency of MoS_2 QDs can be enhanced via atomically dispersed metal modification. DFT calculations show that the introduction of a new defect energy level of Au in the forbidden band of MoS_2 traps extra electrons from the conduction band of n-type MoS_2, passivating multi-particle non-radiative surface states, which increases the recombination probability of conduction band electrons with valence band holes of MoS_2 to enhance the fluorescence efficiency of MoS_2 QDs. The applicability of this mechanism could be further broadened by using electron donors or acceptors to change the electronic state density of single-atom metals modified on other luminescent nanomaterial carriers. The present single-atom metal strategy would expand the applicability of atomically dispersed metal modified luminescent nanomaterials in various fields of optoelectronics devices, clinical diagnosis and bioimaging.

Acknowledgements

This work was supported by the National Key Research and Development Program of China (2017YFA0700500, 2020YFA0406104), the National Natural Science Foundation of China (21635004, 22073045, 21327902), the Excellent Research Program of Nanjing University (ZYJH004), and the Fundamental Research Funds for the Central Universities. We also thank the Electrical Engineering Experimental Center (EEEC) of Shanghai Jiaotong University (SJTU) for HAADF-STEM Facility.

Conflict of Interest

The authors declare no conflict of interest.

Data Availability Statement

The data that support the findings of this study are available in the supplementary material of this article.

Keywords: Atomically Dispersed Metals · Fluorescence Enhancement · Molybdenum Disulfide · Non-Radiative Recombination · Quantum Dots

[1] A. P. Alivisatos, A. L. Harris, N. J. Levinos, M. L. Steigerwald, L. E. Brus, *J. Chem. Phys.* **1988**, *89*, 4001–4011.
[2] V. I. Klimov, A. A. Mikhailovsky, S. Xu, A. Malko, J. A. Hollingsworth, C. A. Leatherdale, H. J. Eisler, M. G. Bawendi, *Science* **2000**, *290*, 314–317.
[3] J. Jung, C. H. Lin, Y. J. Yoon, S. T. Malak, Y. X. Zhai, E. L. Thomas, V. Vardeny, V. V. Tsukruk, Z. Q. Lin, *Angew. Chem. Int. Edit.* **2016**, *55*, 5071–5075.
[4] F. Pelayo García de Arquer, D. V. Talapin, V. I. Klimov, Y. Arakawa, M. Bayer, E. H. Sargent, *Science* **2021**, *373*, eaaz8541.
[5] R. L. van Metter, R. S. Knox, *Chem. Phys.* **1976**, *12*, 333–340.
[6] Y. B. Band, D. F. Heller, *Phys. Rev. A* **1988**, *38*, 1885–1895.
[7] S. J. Strickler, R. A. Berg, *J. Chem. Phys.* **1962**, *37*, 814–822.
[8] J. M. Elward, A. Chakraborty, *J. Chem. Theory Comput.* **2015**, *11*, 462–471.
[9] E. S. Williams, K. J. Major, A. Tobias, D. Woodall, V. Morales, C. Lippincott, P. J. Moyer, M. Jones, *J. Phys. Chem. C* **2013**, *117*, 4227–4237.
[10] J. L. He, A. S. Vasenko, R. Long, O. V. Prezhdo, *J. Phys. Chem. Lett.* **2018**, *9*, 1872–1879.
[11] J. Moreira, B. Serrano, A. Ortiz, H. de Lasa, *Ind. Eng. Chem. Res.* **2010**, *49*, 10524–10534.
[12] Y. J. Wei, Y. M. He, M. C. Chen, Y. N. Hu, Y. He, D. Wu, C. Schneider, M. Kamp, S. Hofling, C. Y. Lu, J. W. Pan, *Nano Lett.* **2014**, *14*, 6515–6519.
[13] T. Senden, F. T. Rabouw, A. Meijerink, *ACS Nano* **2015**, *9*, 1801–1808.

[14] H. Uratani, T. Yoshikawa, H. Nakai, *J. Chem. Theory Comput.* **2021**, *17*, 1290–1300.
[15] M. Zhao, Z. G. Xia, X. X. Huang, L. X. Ning, R. Gautier, M. S. Molokeev, Y. Y. Zhou, Y. C. Chuang, Q. Y. Zhang, Q. L. Liu, K. R. Poeppelmeier, *Sci. Adv.* **2019**, *5*, eaav0363.
[16] X. Wang, H. F. Shi, H. L. Ma, W. P. Ye, L. L. Song, J. Zan, X. K. Yao, X. Y. Ou, G. H. Yang, Z. Zhao, M. Singh, C. Y. Lin, H. Wang, W. Y. Jia, Q. Wang, J. H. Zhi, C. M. Dong, X. Y. Jiang, Y. A. Tang, X. J. Xie, Y. Yang, J. P. Wang, Q. S. Chen, Y. Wang, H. H. Yang, G. Q. Zhang, Z. F. An, X. G. Liu, W. Huang, *Nat. Photonics* **2021**, *15*, 187–192.
[17] R. de Boëver, A. Langlois, X. Li, J. P. Claverie, *JACS Au* **2021**, *1*, 843–851.
[18] I. Hod, V. Gonzalez-Pedro, Z. Tachan, F. Fabregat-Santiago, I. Mora-Sero, J. Bisquert, A. Zaban, *J. Phys. Chem. Lett.* **2011**, *2*, 3032–3035.
[19] B. Pradhan, S. Das, J. X. Li, F. Chowdhury, J. Cherusseri, D. Pandey, D. Dev, A. Krishnaprasad, E. Barrios, A. Towers, A. Gesquiere, L. Tetard, T. Roy, J. Thomas, *Sci. Adv.* **2020**, *6*, eaay5225.
[20] L. C. Liu, A. Corma, *Chem. Rev.* **2018**, *118*, 4981–5079.
[21] L. C. Liu, D. M. Meira, R. Arenal, P. Concepcion, A. V. Puga, A. Corma, *ACS Catal.* **2019**, *9*, 10626–10639.
[22] Y. Shi, C. Lee, X. Y. Tan, L. Yang, Q. Zhu, X. Loh, J. W. Xu, Q. Y. Yan, *Small Struct.* **2022**, *3*, 2100185.
[23] X. N. Li, L. H. Liu, X. Y. Ren, J. J. Gao, Y. Q. Huang, B. Liu, *Sci. Adv.* **2020**, *6*, eabb6833.
[24] D. W. Su, J. Ran, Z. W. Zhuang, C. Chen, S. Z. Qiao, Y. D. Li, G. X. Wang, *Sci. Adv.* **2020**, *6*, eaaz8447.
[25] A. A. Scherbovich, S. A. Maskevich, P. V. Karpach, G. T. Vasilyuk, V. I. Stsiapura, O. V. Venidiktova, A. O. Ayt, V. A. Barachevsky, A. A. Khuzin, A. R. Tuktarov, M. V. Artemyev, *J. Phys. Chem. C* **2020**, *124*, 27064–27070.
[26] J. S. Li, Y. Tang, Z. T. Li, X. R. Ding, B. H. Yu, L. W. Lin, *ACS Appl. Mater. Interfaces* **2019**, *11*, 18808–18816.
[27] K. A. Kuttiyiel, K. Sasaki, Y. M. Choi, D. Su, P. Liu, R. R. Adzic, *Energy Environ. Sci.* **2012**, *5*, 5297–5304.
[28] X. P. Ren, L. Q. Pang, Y. X. Zhang, X. D. Ren, H. B. Fan, S. Z. Liu, *J. Mater. Chem. A* **2015**, *3*, 10693–10697.
[29] B. L. Li, H. L. Zou, L. Lu, Y. Yang, J. L. Lei, H. Q. Luo, N. B. Li, *Adv. Funct. Mater.* **2015**, *25*, 3541–3550.
[30] Y. Shi, T. T. Zhai, Y. Zhou, W. X. Xu, D. R. Yang, F. B. Wang, X. H. Xia, *J. Electroanal. Chem.* **2018**, *819*, 442–446.
[31] Y. Shi, W. M. Huang, J. Li, Y. Zhou, Z. Q. Li, Y. C. Yin, X. H. Xia, *Nat. Commun.* **2020**, *11*, 4558.
[32] S. Das, R. Ghosh, P. Routh, A. Shit, S. Mondal, A. Panja, A. K. Nandi, *ACS Appl. Nano Mater.* **2018**, *1*, 2306–2316.
[33] D. Y. Zhang, D. G. Truhlar, *J. Chem. Theory Comput.* **2020**, *16*, 4416–4428.
[34] I. Lopez-Salido, D. C. Lim, R. Dietsche, N. Bertram, Y. D. Kim, *J. Phys. Chem. B* **2006**, *110*, 1128–1136.
[35] X. L. Yan, S. Li, J. H. Bao, N. Zhang, B. B. Fan, R. F. Li, X. G. Liu, Y. X. Pan, *ACS Appl. Mater. Interfaces* **2016**, *8*, 17060–17067.
[36] D. A. Konopka, M. Li, K. Artyushkova, N. Marinkovic, K. Sasaki, R. Adzic, T. L. Ward, P. Atanassov, *J. Phys. Chem. C* **2011**, *115*, 3043–3056.
[37] K. Samson, M. Sliwa, R. P. Socha, K. Gora-Marek, D. Mucha, D. Rutkowska-Zbik, J. F. Paul, M. Ruggiero-Mikolajczyk, R. Grabowski, J. Sloczynski, *ACS Catal.* **2014**, *4*, 3730–3741.
[38] N. Lehnert, F. Tuczek, *Inorg. Chem.* **1999**, *38*, 1659–1670.
[39] R. X. Jin, C. Liu, S. Zhao, A. Das, H. Z. Xing, C. Gayathri, Y. Xing, N. L. Rosi, R. R. Gil, R. C. Jin, *ACS Nano* **2015**, *9*, 8530–8536.
[40] J. T. Petty, J. Zheng, N. V. Hud, R. M. Dickson, *J. Am. Chem. Soc.* **2004**, *126*, 5207–5212.
[41] K. Kratzl, T. Kratky, S. Gunther, O. Tomanec, R. Zboril, J. Michalicka, J. M. Macak, M. Cokoja, R. A. Fischer, *J. Am. Chem. Soc.* **2019**, *141*, 13962–13969.
[42] S. Maity, D. Bain, A. Patra, *J. Phys. Chem. C* **2019**, *123*, 2506–2515.
[43] P. Li, D. Zhang, Y. C. Zhang, W. Lu, J. W. Zhang, W. Q. Wang, Q. S. He, P. Theato, T. Chen, *ACS Macro Lett.* **2019**, *8*, 937–942.
[44] D. Maity, C. Bhaumik, S. Karmakar, S. Baitalik, *Inorg. Chem.* **2013**, *52*, 7933–7946.
[45] A. Thomas, K. B. Jinesh, *ACS Omega* **2022**, *7*, 6531–6538.
[46] K. F. Mak, K. L. He, C. Lee, G. H. Lee, J. Hone, T. F. Heinz, J. Shan, *Nat. Mater.* **2013**, *12*, 207–211.
[47] C. Galland, Y. Ghosh, A. Steinbruck, M. Sykora, J. A. Hollingsworth, V. I. Klimov, H. Htoon, *Nature* **2011**, *479*, 203–207.
[48] J. Jasieniak, M. Califano, S. E. Watkins, *ACS Nano* **2011**, *5*, 5888–5902.
[49] A. Shirakov, Z. Burshtein, Y. Shimony, E. Frumker, A. A. Ishaaya, *Sci. Rep.* **2019**, *9*, 18810.
[50] J. P. Liu, H. H. Zhou, J. T. Huang, Z. Y. Huang, F. Y. Zeng, Y. F. Kuang, *Int. J. Hydrogen Energy* **2012**, *37*, 16764–16769.
[51] H. Liu, D. Grasseschi, A. Dodda, K. Fujisawa, D. Olson, E. Kahn, F. Zhang, T. Y. Zhang, Y. Lei, R. B. N. Branco, A. L. Elias, R. C. Silva, Y. T. Yeh, C. M. Maroneze, L. Seixas, P. Hopkins, S. Das, C. J. S. de Matos, M. Terrones, *Sci. Adv.* **2020**, *6*, eabc9308.
[52] M. G. Li, J. D. Yao, X. X. Wu, S. C. Zhang, B. R. Xing, X. Y. Niu, X. Y. Yan, Y. Yu, Y. L. Liu, Y. W. Wang, *ACS Appl. Mater. Interfaces* **2020**, *12*, 6276–6282.
[53] S. B. Liu, *J. Phys. Chem. A* **2015**, *119*, 3107–3111.

Manuscript received: May 18, 2022
Accepted manuscript online: June 27, 2022
Version of record online: July 13, 2022